Combustion and Flame 157 (2010) 1906–1915

Contents lists available at ScienceDirect

Combustion and Flame

journal homepage: www.elsevier.com/locate/combustflame

Flame propagation enhancement by plasma excitation of oxygen. Part I: Effects of O_3

Timothy Ombrello [a,*], Sang Hee Won [a], Yiguang Ju [a], Skip Williams [b,1]

[a] Department of Mechanical and Aerospace Engineering, Engineering Quadrangle, Olden Street, Princeton, NJ 08544, USA
[b] Air Force Research Laboratory, Propulsion Directorate, 1950 Fifth Street, Wright-Patterson AFB, OH 45433, USA

ARTICLE INFO

Article history:
Received 23 November 2009
Received in revised form 5 February 2010
Accepted 5 February 2010
Available online 10 March 2010

Keywords:
Plasma-assisted combustion
Ozone
Flame propagation enhancement
Flame speed enhancement
Lifted flame
Tribrachial flame

ABSTRACT

The thermal and kinetic effects of O_3 on flame propagation were investigated experimentally and numerically by using $C_3H_8/O_2/N_2$ laminar lifted flames. Ozone produced by a dielectric barrier plasma discharge was isolated and measured quantitatively by using absorption spectroscopy. Significant kinetic enhancement by O_3 was observed by comparing flame stabilization locations with and without O_3 production. Experiments at atmospheric pressures showed an 8% enhancement in the flame propagation speed for 1260 ppm of O_3 addition to the O_2/N_2 oxidizer. Numerical simulations showed that the O_3 decomposition and reaction with H early in the pre-heat zone of the flame produced O and OH, respectively, from which the O reacted rapidly with C_3H_8 and produced additional OH. The subsequent reaction of OH with the fuel and fuel fragments, such as CH_2O, provided chemical heat release at lower temperatures to enhance the flame propagation speed. It was shown that the kinetic effect on flame propagation enhancement by O_3 reaching the pre-heat zone of the flame for early oxidation of fuel was much greater than that by the thermal effect from the energy contained within O_3. For non-premixed laminar lifted flames, the kinetic enhancement by O_3 also induced changes to the hydrodynamics at the flame front which provided additional enhancement of the flame propagation speed. The present results will have a direct impact on the development of detailed plasma-flame kinetic mechanisms and provided a foundation for the study of combustion enhancement by $O_2(a^1\Delta_g)$ in part II of this investigation.

1. Introduction

Operation at high energy efficiencies with reduced emissions and in restrictive combustion environments necessitates the development of methods to enhance and control combustion processes. Some of the common applications that motivate the development of new technologies to enhance combustion are in systems utilizing advanced gas turbines, pulse detonation engines, and other high-speed air-breathing propulsion devices. But the need goes far beyond high-speed propulsion devices to include stationary power generation and ultra-lean, ultra-low emission internal combustion engines. The above mentioned systems have created environments that push the limits of traditional combustion techniques. There can be a mismatch in the characteristic flow residence time, transport or diffusion time, and the chemical reaction time. Furthermore, the flow speeds can be significantly faster than any deflagration wave velocity, and the transport and diffusion times longer than the ignition delay times. Therefore, to achieve successful ignition, flame propagation, flame stabilization, and complete combustion, there needs to be additional energy and/or active species injection to the system to accelerate the fuel oxidation processes. Consequently, the exploration of new methods to reduce chemical reaction times has attracted much attention. New combustion technologies, such as plasma-assisted combustion, have shown much promise to enhance both thermally and kinetically the ignition, flame stabilization, and flame propagation in combustion systems and therefore require a fundamental understanding of the underlying enhancement mechanisms.

It is well known from the Arrhenius expression that chemical reaction rates can be accelerated by either increasing the pre-exponential factor, A, the temperature, T, or decreasing the activation energy, E_a

$$k \approx Ae^{-E_a/T}. \quad (1)$$

Thermal enhancement through elevated temperatures is well known and accelerates the rate of fuel oxidation for endothermic processes, but can be costly because of having to increase the translational energy of all molecules in the system. Kinetic enhancement by increasing the pre-exponential factor or decreasing the activation energy is more selective. Instead of supplying en-

* Corresponding author. Present address: Air Force Research Laboratory, Propulsion Directorate, 1950 Fifth Street, Building 18 D, Room D229, Wright-Patterson AFB, OH 45433, USA. Fax: +1 937 656 4659.
E-mail addresses: timothy.ombrello@wpafb.af.mil (T. Ombrello), sangwon@princeton.edu (S.H. Won), yju@princeton.edu (Y. Ju), skip.williams@maui.afmc.af.mil (S. Williams).
[1] Present address: Air Force Research Laboratory, Directed Energy Directorate, Detachment 15, 535 Lipoa Parkway, Suite 200, Kihei, Maui, Hawaii 96753, USA.

0010-2180/$ - see front matter © 2010 The Combustion Institute. Published by Elsevier Inc. All rights reserved.
doi:10.1016/j.combustflame.2010.02.005

Report Documentation Page

Form Approved
OMB No. 0704-0188

1. REPORT DATE	2. REPORT TYPE	3. DATES COVERED
10 MAR 2010		**00-00-2010 to 00-00-2010**

4. TITLE AND SUBTITLE	5a. CONTRACT NUMBER
Flame propagation enhancement by plasma excitation of oxygen. Part I: Effects of O3	5b. GRANT NUMBER
	5c. PROGRAM ELEMENT NUMBER
6. AUTHOR(S)	5d. PROJECT NUMBER
	5e. TASK NUMBER
	5f. WORK UNIT NUMBER
7. PERFORMING ORGANIZATION NAME(S) AND ADDRESS(ES) **Princeton University,Department of Mechanical and Aerospace Engineering,Princeton,NJ,08544**	8. PERFORMING ORGANIZATION REPORT NUMBER
9. SPONSORING/MONITORING AGENCY NAME(S) AND ADDRESS(ES)	10. SPONSOR/MONITOR'S ACRONYM(S)
	11. SPONSOR/MONITOR'S REPORT NUMBER(S)

12. DISTRIBUTION/AVAILABILITY STATEMENT
Approved for public release; distribution unlimited

13. SUPPLEMENTARY NOTES

14. ABSTRACT

The thermal and kinetic effects of O3 on flame propagation were investigated experimentally and numerically by using C3H8/O2/N2 laminar lifted flames. Ozone produced by a dielectric barrier plasma discharge was isolated and measured quantitatively by using absorption spectroscopy. Significant kinetic enhancement by O3 was observed by comparing flame stabilization locations with and without O3 production. Experiments at atmospheric pressures showed an 8% enhancement in the flame propagation speed for 1260 ppm of O3 addition to the O2/N2 oxidizer. Numerical simulations showed that the O3 decomposition and reaction with H early in the pre-heat zone of the flame produced O and OH, respectively, from which the O reacted rapidly with C3H8 and produced additional OH. The subsequent reaction of OH with the fuel and fuel fragments, such as CH2O, provided chemical heat release at lower temperatures to enhance the flame propagation speed. It was shown that the kinetic effect on flame propagation enhancement by O3 reaching the pre-heat zone of the flame for early oxidation of fuel was much greater than that by the thermal effect from the energy contained within O3. For non-premixed laminar lifted flames, the kinetic enhancement by O3 also induced changes to the hydrodynamics at the flame front which provided additional enhancement of the flame propagation speed. The present results will have a direct impact on the development of detailed plasma-flame kinetic mechanisms and provided a foundation for the study of combustion enhancement by O2(a1Dg) in part II of this investigation.

15. SUBJECT TERMS

16. SECURITY CLASSIFICATION OF:			17. LIMITATION OF ABSTRACT	18. NUMBER OF PAGES	19a. NAME OF RESPONSIBLE PERSON
a. REPORT **unclassified**	b. ABSTRACT **unclassified**	c. THIS PAGE **unclassified**	**Same as Report (SAR)**	**10**	

Nomenclature

a	density ratio between the fuel and oxidizer (ρ_F/ρ_∞)
A	pre-exponential factor
d	diameter of the fuel nozzle
E_a	activation energy
FWHM	full-width half-maximum
I	intensity of light with the presence of ozone
I_0	intensity of light without the presence of ozone
k	reaction rate coefficient
L	absorption path length
N_{ozone}	number density of ozone
ppm	parts per million
r	radial distance from the centerline
r_0	radius of the fuel nozzle
Re	Reynolds number
S_{lifted}	lifted flame speed
$S_{laminar}$	laminar flame speed
Sc	Schmidt number
T	temperature
u	local flow velocity
u_0	initial fuel jet velocity
V_{co}	co-flow velocity
x	distance from fuel nozzle tip
X	non-dimensional axial distance
X_v	virtual origin for velocity
$X_{v,F}$	virtual origin for concentration
Y_F	fuel concentration
v_∞	kinematic viscosity
$\rho_{unburned}$	density of unburned gas
ρ_{burned}	density of burned gas
ρ_F	density of fuel
ρ_∞	density of oxidizer
σ_{ozone}	absorption cross section of ozone

ergy to a system to elevate the temperature, energy can be used to create active species to change reaction pathways for higher efficiencies. This type of kinetic enhancement has been focused traditionally on catalysts and additives that could be injected into the system to react more rapidly [1–3] as well as using pre-combustion [4,5]. Therefore, combustion enhancement through selective kinetic processes, especially with in situ species production, has great potential with regard to energy efficiency concerns for practical applications.

Compared to catalysts and additives, plasma activation offers a rapid and promising method to thermally and kinetically enhance combustion processes with in situ production of active species for more rapid fuel oxidation. Plasma can couple energy into combustion systems to produce radicals, excited species, ions, and electrons as well as elevated temperatures. The production of new species can alter the chemical potential of the fuel and/or oxidizer to react more rapidly and enhance the overall combustion process. Simultaneously, the elevated temperatures from the plasma can also aid in the combustion reaction process where radical quenching at low temperatures are too large.

Because of the significant potential of plasma, much research has been performed using a variety of plasma discharge systems including plasma torches/jets [6–9], gliding arc discharges [10–12], fast ionization waves [13,14], and nanosecond repetitively pulsed discharges [15,16], as well as through electric field interactions [17–19], microwave discharges [20–23], and many others. The investigations have shown definitively that plasma can enhance combustion processes with decreased ignition times and lower ignition temperatures [10,11,15,16,24,25], increased flame propagation [18,19,21–23], enhanced flame stabilization, and extended flammability limits [7,8,12,20]. It has been stated in a recent review of plasma-assisted combustion that "artificial initiation of chemical chains by low temperature plasma of gas discharges does exist," but there is a lack of data from controlled and well-defined experiments [26].

Plasma can couple energy into combustion systems via many different pathways producing a diverse range and significant number of species including radicals, excited species, ions, and electrons (Fig. 1). The inclusion of each and every species and their associated reactions would render kinetic mechanisms nearly impossible to use. More importantly, there is a lack of understanding of what species and reaction pathways are the most important. Therefore, one of the greatest challenges that remain for developing a clear understanding of plasma-assisted combustion is a fundamental knowledge of specific enhancement processes. Once the individual enhancement pathways are understood, detailed plasma-flame kinetic mechanisms can be developed for quantitative prediction and optimization of practical combustion systems to achieve increased energy conversion efficiency and reduced emissions.

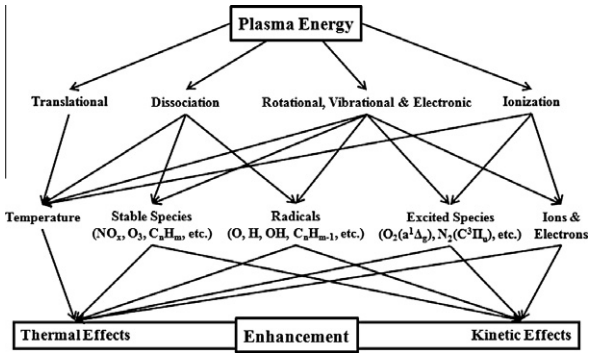

Fig. 1. Pathways of enhancement from plasma-coupled energy to combustion systems.

One of the most challenging issues in experiments of plasma-assisted combustion is to isolate the individual effects of different species and processes so that the effect of each reaction pathway can be quantitatively determined. However, isolating the individual enhancement mechanisms by each species can be difficult because plasma-assisted combustion systems are highly coupled with complex hydrodynamics, species diffusion and mixing, and thermal processes. The coupled processes render an understanding of the underlying physics and chemical processes difficult. Furthermore, there exists the additional complication of the different lifetime scales of plasma-produced species when trying to observe individual enhancement pathways.

The first steps to decouple the plasma-flame kinetic process are to examine the critical species. In air, there will be plasma production of oxygen containing species such as O, O_3, O_2(v), O(^{1}D), O(^{1}S), $O_2(a^1\Delta_g)$, $O_2(b^1\Sigma_g)$, as well as other excited species, ions, and electrons. The nitrogen containing species include N, NO, NO_2, N(^{4}S), N_2(v), $N_2(A^3\Sigma_u)$, $N_2(B^3\Pi_g)$, $N_2(a'^1\Sigma_u)$, $N_2(a^1\Pi_g)$, $N_2(C^3\Pi_u)$, $N_2(a''^1\Sigma_g)$, N(^{2}D), N(^{2}P), and multiple ions, etc. [27]. These species do not take into account species produced by plasma discharge of the fuel. Therefore, it can be difficult to identify the most important species and reaction pathways in a premixed fuel and oxidizer system.

Nevertheless, the specific kinetic enhancement pathways through catalytic effects of plasma-produced NO_x have been established [10,11]. The results showed that the NO_x catalytic effects via HO_2 and CH_3O_2 dramatically lowered the ignition temperature and suppressed the inhibitive effects of H_2O and CH_4. Additionally, plasma-produced radical species such as O, OH, and excited species have been shown to be in significant concentrations in plasma-assisted combustion systems to enhance reaction processes. A recent study by Uddi et al. found significant ignition enhancement using a pulsed nanosecond discharge with quantitative measurements of the time dependent production and decay of atomic oxygen after the discharge in a premixture [28]. The time dependent production and decay of OH was also measured with ignition enhancement observed [24]. However, the effects of plasma generated long-lifetime species such as O_3 and $O_2(a^1\Delta_g)$ (radiative lifetime in excess of 4000 s at 300 K [29]) on combustion have not been investigated quantitatively. In addition, these two species are often coupled in the afterglow of non-equilibrium plasma. Therefore, their individual effects on combustion enhancement have to be understood via a successful decoupling of $O_2(a^1\Delta_g)$ from O_3.

Unfortunately, there has been little experimental work emphasizing the combustion enhancement effects by O_3 and $O_2(a^1\Delta_g)$. Early experimental studies of the effect of O_3 on ignition delay times were conducted in compression and spark ignition engines [30–34]. Recently, laser ignition has also been investigated by using both CO_2 and KrF excimer lasers to excite and decompose O_3 [35–37]. To the authors' knowledge, there have only been two investigations of the effect of O_3 on flame propagation enhancement [32,38]. Although these experiments reported the flame speed enhancement by O_3, the exact mechanisms are not well understood. Moreover, quantification of the enhancement was difficult due to the complex experimental geometry.

The goal of the present work was to create a methodology to isolate and quantitatively measure the effects of specific plasma-excited oxygen species on the enhancement of flame propagation at a pressure of 101.3 kPa. In the current work, the enhancement of flame propagation by O_3 was investigated through the development of an integrated plasma-combustion experimental platform where the species were produced, isolated, transported, and quantitative measurements taken through absorption spectroscopy. A low power dielectric barrier discharge plasma was used to activate O_2 and produce O_3, which was merged with N_2 for the oxidizer co-flow of atmospheric pressure C_3H_8 lifted flames. The experimental results were compared to numerical simulations to identify the important kinetic pathways of flame propagation enhancement in the plasma-flame systems and provide important steps towards developing a comprehensive and predictive model for the inclusion of other plasma-produced species, such as the work on $O_2(a^1\Delta_g)$ in part II of this investigation.

2. Experimental system

2.1. Plasma-assisted lifted flames

A laminar lifted flame burner was adopted for the combustion platform and used at a pressure of 101.3 kPa for all experiments. A schematic of the platform is shown in Fig. 2. The lifted flame burner consisted of a central fuel jet with an inner diameter of 0.271 mm that was located in a 90 mm inner diameter fused silica (quartz) tube to contain the co-flow of oxidizer. The fuel nozzle was aerodynamically shaped to produce a uniform velocity profile at the exit. The large ratio of diameters between the oxidizer co-flow and the fuel jet (>100) were used to ensure accurate comparisons to similarity solutions of the flow field (to be described in Section 3.1). To ensure that the co-flow was uniform, two stainless steel meshes coated with silica for chemical inertness were separated by 3 cm and were located between the oxidizer inlet of the burner and the fuel jet exit. The gases used in the experiments

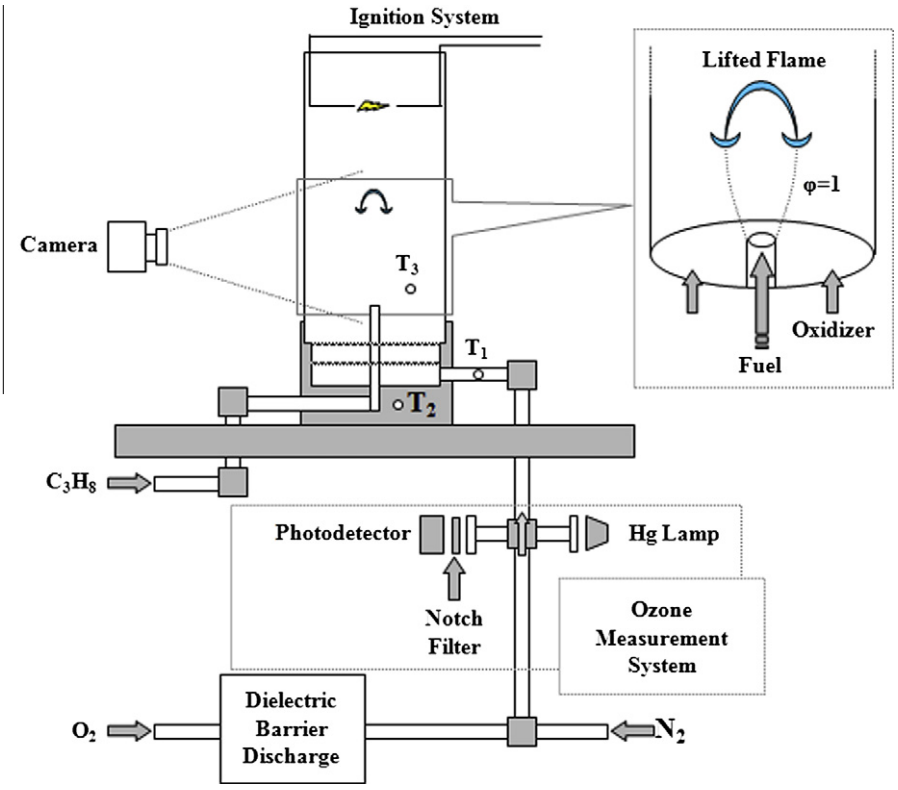

Fig. 2. Experimental set-up schematic of the lifted flame burner integrated with a dielectric barrier plasma discharge device and O_3 absorption measurement system.

were C_3H_8 for the fuel and ultra-high purity O_2 (99.99%) and N_2 (99.95%) mixed for the oxidizer. The flow rate of the fuel was controlled with a calibrated mass flow meter while the O_2 and N_2 were controlled with calibrated sonic nozzles. The undiluted ultra-high purity O_2 was passed through a dielectric barrier discharge device and was then merged with the N_2 stream to be introduced to the lifted flame burner. This configuration minimized any problems of NO_x being produced in the discharge which would contaminate the flow. The dielectric barrier discharge device was comprised of a 110 mm long and 18 mm diameter co-axial sleeved tube geometry with a gap distance of 2 mm. The power was supplied by pulses of 3–10 kV positive and negative polarities with duration of 10 ns at FWHM with a frequency varied between 10 kHz and 40 kHz to produce different O_3 concentrations. Each pulse contained between 0.1 mJ and 1 mJ, providing between 1 W and 40 W total power. The discharge produced multiple oxygen containing species including O, O_3, O_2(v), $O(^1D)$, $O(^1S)$, $O_2(a^1\Delta_g)$, $O_2(b^1\Sigma_g)$, etc. To ensure that O_3 was the only species present in the flow when merged with the N_2 stream, a sufficient residence time was given to quench all plasma-produced species other than O_3. For example, Table 1 lists the quenching rates of some of the common plasma-produced oxygen species. The atomic oxygen rapidly recombines with O_2 to produce O_3, which is stable. The next longest lived species is $O_2(a^1\Delta_g)$ which is metastable, and at 101.3 kPa and 300 K has a collisional lifetime of approximately 20 ms. With the flow rate and length of the tube between the dielectric barrier discharge and the merging with N_2 the residence time was over 100 ms. Therefore, when the dielectric barrier discharge was supplied with power, the only change in the gases entering the combustion system would be the addition of O_3.

The high velocity fuel jet (3.5–10 m/s) and low velocity oxidizer co-flow (0.049 m/s) created a flow field with a stoichiometric contour where the premixed flame head of a lifted flame was located (shown in the top right inset in Fig. 2). The lifted flame, which is also called a tribrachial (triple) flame, had a premixed flame head anchored on the stoichiometric contour, followed by a diffusion flame tail. Photographs of the flame at various liftoff heights are shown in Fig. 3. The lifted flame could be located at different stationary distances from the fuel jet nozzle depending upon the local flow velocity. For a fixed flow field, the flame is located in a stationary position where the lifted flame speed at the premixed flame head is balanced with the local flow velocity. If the flame speed increases, the liftoff height decreases to re-establish a local dynamic balance between the flame speed and flow velocity. A plot of the flame liftoff height versus fuel jet velocity is shown in Fig. 4.

Due to the slow laminar boundary layer development and the velocity and concentration gradients created, the lifted flame height is very sensitive to the changes in flame speed and therefore provides excellent flame geometry for the direct observation of flame speed enhancement. For example, with only a small concentration of O_3, the flame liftoff height changes appreciably, as shown in Fig. 4. Since the fuel and oxidizer are not mixed far upstream of the flame, there is very short residence time for the fuel and oxidizer to react in the cold flow. The short residence time helps to further decouple the enhancement effects to be directly from reactions in the flame zone and not far upstream in the cold un-reacted flow.

Table 1
Reaction rates of plasma-produced oxygen species at 298 K. The term "HP" refers to the high pressure limit.

Reaction	Reaction constant (cm^3/molecule/s)
$O + O_2 + M \rightarrow O_3 + M$	6.0×10^{-34} = (HP limit 3.61×10^{-10}) [39]
$O(^1D) + O_2 \rightarrow O + O_2$	4.0×10^{-11} [39]
$O_2(v) + O_2 \rightarrow O_2 + O_2$	1.73×10^{-13} [40]
$O_2(b^1\Sigma_g) + O_2 \rightarrow O_2 + O_2$	4.1×10^{-17} [39]
$O_2(a^1\Delta_g) + O_2 \rightarrow O_2 + O_2$	1.6×10^{-18} [39]
$O_2(a^1\Delta_g) + Ar \rightarrow O_2 + Ar$	1.0×10^{-20} [41]

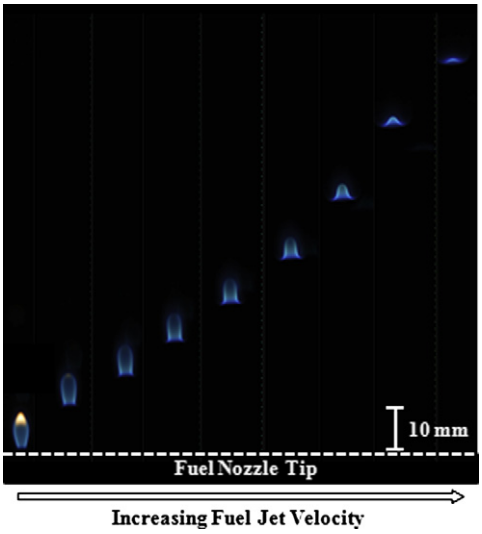

Fig. 3. Photographs of lifted flames at stationary positions for different fuel jet velocities.

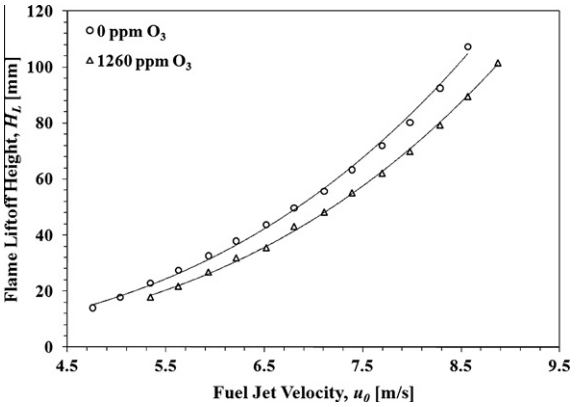

Fig. 4. Measurements of the flame liftoff height as a function of fuel jet velocity showing different flame stabilization locations from Fig. 3, as well as the sensitivity of flame speed changes.

Multiple temperatures were monitored by thermocouples placed on flow surfaces and in the flow and were recorded in the system. Temperatures were measured at points T_1, T_2, and T_3 shown in Fig. 2 and were respectively the burner inlet tube surface temperature, burner surface temperature, and co-flow gas temperature. Throughout the experiments, the temperatures remained constant within 0.2 K between the plasma being turned on and off.

2.2. Quantitative absorption measurements of O_3

The O_3 produced by the dielectric barrier discharge was measured using a one-pass, line-of-sight absorption cell in the flow downstream of where the O_2 and N_2 streams merged. The absorption cell was comprised of a stainless steel compression cross fitting with the side arms made of quartz tubes capped with UV quality windows. The cell was placed in the flow between the merging of O_2 and N_2 streams and the burner. At one window, a mercury light with stable output provided ultraviolet light at the wavelength of 253.7 nm where O_3 has a peak absorption cross section of 1.137×10^{-17} cm^2 (at 300 K) in the Hartley band [42]. A

10 nm notch filter (isolating only the 253.7 nm mercury line) and a photodiode detector were placed at the exit of the transmission cell. No other species present in the flow (O_2 and N_2) absorb at this wavelength. Therefore, the change in the transmittance of the cell with the plasma on and off could be used to determine the O_3 concentration through the Beer–Lambert law

$$N_{ozone} = \frac{-\ln(\frac{I}{I_0})}{\sigma_{ozone} L}, \quad (2)$$

where N_{ozone} is the absolute number density of the absorbing species, O_3, I the intensity of light with the presence of O_3, I_0 the intensity of light without the presence of O_3, σ_{ozone} the absorption cross section of O_3 at the excitation wavelength of 253.7 nm, and L the path length in the absorption cell (12.48 cm). The concentration was then calculated in parts per million (ppm) of O_3 with an uncertainty of approximately ±2% and a minimum detectable threshold of approximately 15 ppm. The uncertainty and minimum detectable threshold came from the fluctuations in the intensity of the mercury light as a function of time during the experiments.

2.3. Experiment procedures

The O_2 loading was fixed at 18% O_2 in 82% N_2 for the oxidizer co-flow. This O_2 loading was chosen to ensure that the flame was completely within the laminar flow regime for the 0.271 mm diameter fuel nozzle used [43], as well as to maintain a maximum liftoff height well below the location of the igniter. The oxidizer co-flow velocity was fixed at 0.049 m/s and the fuel velocity was small enough to have a nozzle attached diffusion flame when ignited. The flame was photographed by using a high resolution (10.2 megapixel) Nikon D40x camera, then the dielectric barrier discharge was turned on and a photograph taken again of the stationary flame. The fuel velocity was then increased in small increments, where at each increment photographs taken of the flame with the dielectric barrier discharge off and on. This procedure was executed for at least 10 flame liftoff heights between a nozzle attached flame and a flame at the top of the stoichiometric contour. The experimental repeatability of flame liftoff height as a function of fuel jet velocity was carefully tested multiple times. The results showed that the lifted flame co-flow system had deviations in the flame liftoff height that were negligibly small at less than 1 mm.

For each condition where the dielectric barrier discharge was on, the O_3 concentration was measured in the absorption cell. To ensure that the O_3 measured in the absorption cell was the concentration that was present at the flame front, the experiments were performed with the absorption cell at different distances and flow residence times between the merging of the O_2 and N_2 and measuring location, as well as between the measuring location and the flame. There was no change in the O_3 concentration measured and/or a change in the flame enhancement by O_3, confirming that the O_3 concentration measured in the absorption cell was the concentration present at the flame.

3. Results and discussion

3.1. Effects of O_3 addition on lifted flame height

The lifted flame was established for fixed oxidizer co-flow velocity and O_2 loading (18% O_2 in 82% N_2). The fuel jet velocity was increased and pictures were taken at each stationary flame condition with and without O_3 present in the oxidizer (Fig. 3). More than 10 fuel jet velocities were chosen to give a complete data range between a nozzle attached flame and blowout of a lifted flame at the top of the stoichiometric contour. Since the fuel jet velocity was almost a factor of 100 larger than the co-flow velocity and the fuel jet diameter was more than 100 times smaller than the co-flow diameter, a similarity solution was applicable for the cold flow [44]. The similarity solution was used to find where the stoichiometric contour existed and hence where the premixed head of the lifted flame was anchored.

By accounting for the density, the virtual origin, and co-flow velocity for uniform jet velocity profile at the nozzle exit, the local flow velocity, u, and fuel concentration, Y_F, can be derived in terms of the non-dimensional axial distance, X, and radius, R, from the similarity solution in Eqs. (3) and (4), respectively.

$$\frac{u - V_{co}}{u_0 - V_{co}} = a\frac{(1-\frac{q}{a})}{1-q}\frac{3}{32(X - X_v)}\frac{1}{\left[1 + 3a(1-\frac{q}{a})\left(\frac{R}{32(X+X_v)}\right)^2\right]^2} \quad (3)$$

$$Y_F = a(2\mathrm{Sc}+1)\frac{1}{32(X - X_{v,F})}\frac{1}{\left[1 + 3a(1-\frac{q}{a})\left(\frac{R}{32(X+X_{v,F})}\right)^2\right]^{2\mathrm{Sc}}}. \quad (4)$$

The non-dimensional axial distance and radius are defined as $X = x/(d\mathrm{Re})$ and $R = r/r_0$, respectively, where x is the distance from the fuel nozzle tip, r the radial distance from the centerline, d and r_0 the diameter and radius of the fuel nozzle, respectively, Re the Reynolds number defined as $u_0 d/\nu_\infty$, u_0 the initial jet velocity, and ν_∞ the kinematic viscosity (1.574×10^{-5} m^2/s was used, which is for 18% O_2 in 82% N_2 at 101.3 kPa and 300 K). Also, V_{co} is the co-flow velocity, a the density ratio between the fuel and oxidizer ρ_F/ρ_∞, q the ratio between the co-flow velocity and initial jet velocity V_{co}/u_0, Sc the Schmidt number of C_3H_8 (Sc = 1.366) which was the fuel used in the experiments, and X_v and $X_{v,F}$ the virtual origins for velocity and concentration, respectively.

Using both the similarity equation for velocity and concentration, the stoichiometric contour was found and compared with the flame location in the experiments. Fig. 5 shows a plot of the experimental results of flame radius normalized by the nozzle radius at various conditions of fuel jet velocity with and without the presence of O_3 superimposed on a plot of the calculated cold flow stoichiometric contour. The good agreement between the flame radii with and without O_3 addition and the cold flow stoichiometric contour shows that the similarity solution of the flow is representative of the flame location. Furthermore, by assuming a thin flame and neglecting the effect of thermal expansion, the local flow velocities along the stoichiometric contour can be considered comparable to the lifted flame speed. The approximation of a thin reaction zone has been validated in previous experiments [43–47], by showing that the extrapolation of tribrachial flame speed to a

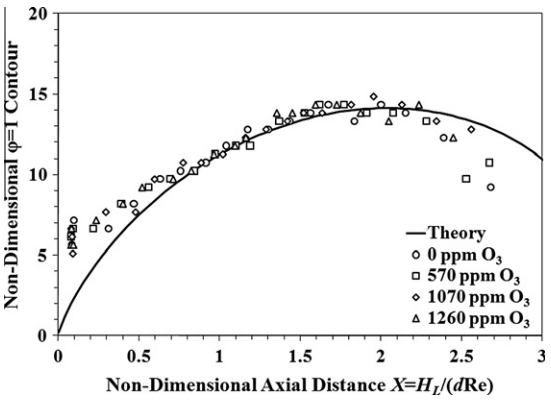

Fig. 5. Plot of stoichiometric contour from the similarity solution and experimentally obtained flame radii.

zero mixture fraction gradient agrees well with the maximum propagation speed of tribrachial flames predicted theoretically [48].

To evaluate the enhancement with O_3 addition, an understanding of the flame stabilization mechanism is required. The stabilization mechanism of laminar lifted flames can be explained based upon the dynamic balance between the local flow velocity and flame speed along the stoichiometric contour. The leading edge of the lifted flame base at the premixed flame head is always located on the stoichiometric contour as shown in Fig. 5 [43]. The spatial profiles of local flow velocity from both similarity solutions with and without the virtual origins are plotted in terms of non-dimensional axial distance, X, in Fig. 6. The flow velocities along the stoichiometric contour with and without the virtual origins are shown to deviate significantly when close to the fuel jet nozzle. Nevertheless, for the range of liftoff height used in the experiments, the deviation between the two solutions is on the order of 1%. Also plotted in Fig. 6 are the lifted flame speeds with and without O_3 addition, which were converted from the measurements of lifted flame heights by varying the initial jet velocity. Normally, without O_3 addition, the lifted flame stabilizes where the local flow velocity on the stoichiometric contour is balanced with the lifted flame speed. When O_3 is added to the system, the flame propagation speed is enhanced and the flame moves upstream to a new stabilization location where there is a dynamic balance. The result in Fig. 6 indicates clearly that the lifted flame is stabilized by the balance between the local flow velocity and flame propagation speed with and without O_3 addition.

The lifted flame speeds were evaluated based upon the axial local flow velocity from the similarity solution of the cold flow at the measured liftoff heights with initial jet velocities. The results are plotted in Fig. 7 as a function of fuel mixture fraction gradient. It is shown clearly that there is an enhancement of the lifted flame speed with increasing O_3 concentration. Interestingly, the enhancement of lifted flame speed increases with increasing fuel mixture fraction gradient for the same concentration of O_3. This can be explained reasonably with a coupling effect between kinetic enhancement and changes to the flame front curvature leading to a hydrodynamic enhancement by considering the unique characteristics of the triple flame structure of laminar lifted flames.

Firstly, numerical simulations were performed for equivalence ratios of 0.8–1.2 with and without 5000 ppm of O_3. This concentration of O_3, which was larger than what was used in the experiments, was chosen in order to demonstrate more clearly what the effect was on the detailed structure of the flame which was not as easily observable numerically for lower O_3 concentrations. The mechanisms of enhancement remain the same regardless of

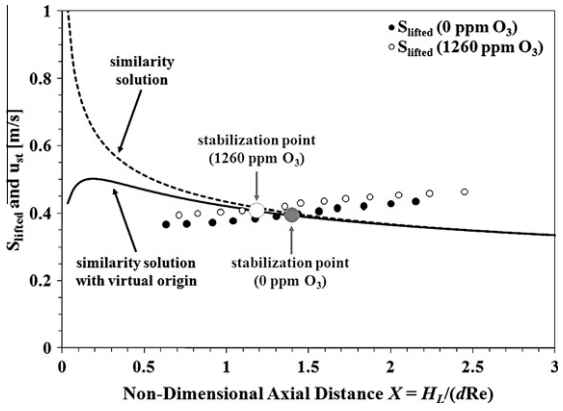

Fig. 6. Plot of the velocities along the stoichiometric contour found from similarity solutions with and without virtual origins along with the lifted flame speed with and without O_3 addition showing the flame stabilization mechanisms.

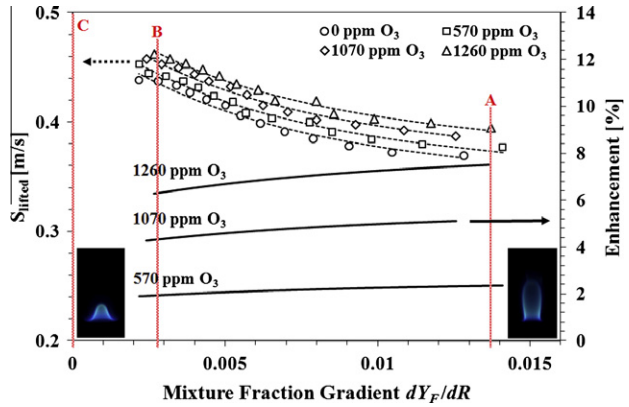

Fig. 7. Plot of the lifted flame speed, S_{lifted}, and percent enhancement of S_{lifted} as a function of mixture fraction gradient at 101.3 kPa with and without O_3 addition. The inset pictures of the lifted flames show the differences in the flame front near the fuel nozzle (right) and far from the fuel nozzle (left).

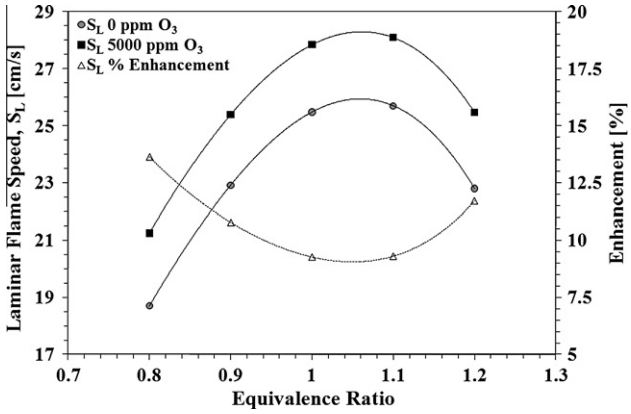

Fig. 8. Plot of the numerical simulation results of laminar flame speed, S_L, enhancement by O_3 as a function of equivalence ratio.

the O_3 concentration. The results in Fig. 8 show that the laminar flame speed is enhanced more for lean and rich equivalence ratios than at stoichiometric. This is reasonable because lean and rich premixed flames have relatively weaker reactivity and lower chemical heat release compared to the stoichiometric condition. Therefore, the off-stoichiometric flame is more sensitive to the same amount of energy input associated with the addition of O_3. The lifted flame speed is also a strong function of the curvature at the premixed flame front [45,46] which is not only coupled with the fuel mixture fraction gradient but also the flow velocity gradient and hence hydrodynamics. The premixed flame curvature of the triple flame structure is determined by the change of laminar flame speed with the equivalence ratio and the upstream flow profile based on the dynamic balance between flame speed and local flow velocity [43]. With O_3 addition to the co-flow of air, the non-uniform enhancement of laminar flame speed with the equivalence ratio induces an increase in the radius of the triple flame front since the lean and rich premixed flame will be enhanced more, as shown in Fig. 8. The larger radius of the flame leads to more significant flow redirection upstream of the flame. Therefore, the local flow velocity at the premixed flame head will decrease and allow for enhanced lifted flame propagation speeds. Consequently, the lifted flame propagation speed is enhanced more by this effect because of the change in curvature of the flame front with O_3 addition.

Secondly, the increase of enhancement with larger mixture fraction gradient can be attributed to the change of velocity gradient in the radial direction when the liftoff height is decreased by

the addition of O_3. Previous work demonstrated experimentally that the triple flame structure of the lifted flame is tilted by the velocity gradient change and the tilting angle is proportionally increased with an increase of the velocity gradient [47]. Thus, when the lifted flame moves to an upstream position because of flame speed enhancement from the addition of O_3, the lifted flame front is subjected to a larger velocity gradient, tilting the flame front further. The effect of the velocity gradient becomes more significant when the lifted flame is at a location closer to the nozzle because the velocity gradient also non-linearly increases with the decrease of the lifted flame height from the fuel jet exit. Consequently, the current evaluation method of lifted flame speed may over-predict the enhancement of lifted flame speed since the axial local flow velocity has been considered only. The detailed effect on flame front geometry changes through tilting, curvature, and stretch are out of scope of current study. However, the flame front geometry changes are extremely important because of the increased flame propagation enhancement beyond the purely kinetic effect. This effect has been termed the kinetic-induced hydrodynamic enhancement.

To exclude the complicated enhancement mechanism caused by the hydrodynamic matters discussed above, and to focus on the kinetic enhancement on the lifted flame speed, the lifted flame speed was extrapolated to a zero mixture fraction gradient. The process allowed for direct comparison with the stoichiometric laminar flame speed. In the limit of zero mixture fraction gradient and flame curvature, the lifted flame speed, S_{lifted}, is related to the laminar flame speed, S_L, through the unburned to burned density ratio [43,48]

$$S_{lifted} \approx S_L \sqrt{\frac{\rho_{unburned}}{\rho_{burned}}}. \tag{5}$$

Therefore, the experimental results of lifted flame speed could be compared to calculated laminar flame speeds.

The enhancement of the local lifted flame speed and the extrapolated lifted flame speed are plotted as a function of O_3 concentration in Fig. 9 together with the numerical simulation results of purely kinetic enhancement. For the simulations with O_3 addition, the O atoms were conserved as to not perturb the total oxidizer fraction in the mixture. Furthermore, the O_3 concentrations were adjusted to the ppm concentrations for a stoichiometric flame instead of what was measured in the O_2 and N_2 mixture. For a large mixture fraction gradient, marked as A in Fig. 7, the enhancement is the largest as shown in Fig. 9. The factor of four difference in the flame speed enhancement between this fuel mixture fraction gradient and the purely kinetic enhancement are indicative of the kinetic-induced hydrodynamic enhancement described earlier in this section. For a small mixture fraction gradient, marked as B in Fig. 7, the local flame speed enhancement is less, approaching the calculated purely kinetic enhancement results. The extrapolation to a zero mixture fraction gradient has been performed with a correlation factor $R > 0.99$ and agreed well with numerical simulation results, marked as C in Fig. 7. Note that the deviation between experimental and numerical results becomes slightly larger for larger O_3 concentration. This effect is once again caused by the kinetic-induced hydrodynamic enhancement for larger concentrations of O_3. Note that the smaller deviation between the extrapolated flame speed enhancement and the purely kinetic enhancement that was calculated is due to the extrapolation process averaging out the hydrodynamic enhancement. The details of the kinetic enhancement mechanism will be discussed in the following section with numerical simulation results.

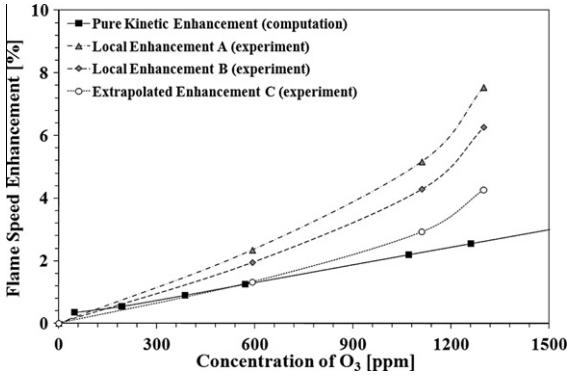

Fig. 9. Plot of experimental results compared to numerical simulations. The local enhancement of "A" and "B" are indicated for large and small mixture fraction gradients, respectively, shown in Fig. 6, while "C" indicates the lifted flame speed enhancement when extrapolated to a zero mixture fraction gradient.

3.2. Computations of laminar flame speed enhancement with O_3 addition

To understand the flame speed enhancement pathways with O_3 addition, numerical simulations were performed using the PREMIX code from the CHEMKIN package [49]. The PREMIX code allows for one-dimensional calculations of laminar flames which can be used along with the relation in (5) to quantify the enhancement of lifted flame speed.

For the kinetic mechanism, the O_3 reactions [50,51] in Table 2 were added to the C_3H_8 mechanism [52]. The two most important reactions were the decomposition reaction of

$$O_3 + M \leftrightarrow O_2 + O + M, \tag{6}$$

and the O atom three body recombination reaction of

$$O + O + M \leftrightarrow O_2 + M \tag{7}$$

because of the production and consumption of O. The reaction of C_3H_8 with O_3 was also added but was not significant in the reaction system. The low impact of this reaction was because the reaction rate was several orders of magnitude slower than the O_3 decomposition reaction [53]. The reaction is slow because O_3 does not react

Table 2
Rate constants for reactions of O_3 [50,51] that were added to the C_3H_8 chemical mechanism [52].

Reaction	Reaction constant (cm^3/mole/s)	Temperature dependence	Activation energy (kJ/mole)
$O_3 + O_2 \rightarrow O_2 + O + O_2$	1.54×10^{14}	0	96.5
$O_3 + O \rightarrow O_2 + O + O$	2.48×10^{15}	0	95.09
$O_3 + O_3 \rightarrow O_2 + O + O_3$	4.40×10^{14}	0	96.5
$O_3 + N_2 \rightarrow O_2 + O + N_2$	4.00×10^{14}	0	94.84
$O_2 + O + O_2 \rightarrow O_3 + O_2$	3.26×10^{19}	−2.1	0
$O_2 + O + N_2 \rightarrow O_3 + N_2$	1.60×10^{14}	−0.4	−5.82
$O_2 + O + O \rightarrow O_3 + O$	2.28×10^{15}	−0.5	−5.82
$O_2 + O + O_3 \rightarrow O_3 + O_3$	1.67×10^{15}	−0.5	−5.82
$O_2 + O_2 \rightarrow O + O + O_2$	9.80×10^{24}	−2.5	493.99
$O_2 + O \rightarrow O + O + O$	3.50×10^{25}	−2.5	493.99
$O_2 + O_3 \rightarrow O + O + O_3$	1.20×10^{19}	−1	493.99
$O_2 + H_2O \rightarrow O + O + H_2O$	1.20×10^{19}	−1	493.99
$O + O + O_2 \rightarrow O_2 + O_2$	1.50×10^{16}	−0.4	0
$O + O + N_2 \rightarrow O_2 + N_2$	6.00×10^{13}	0	−7.49
$O + O + O \rightarrow O_2 + O$	5.34×10^{16}	−0.4	0
$O + O + O_3 \rightarrow O_2 + O_3$	1.30×10^{14}	0	−7.49
$O_2 + O_2 \rightarrow O_3 + O$	1.20×10^{13}	0	420.12
$O_3 + O \rightarrow O_2 + O_2$	4.82×10^{12}	0	17.14
$O_3 + H \rightarrow O_2 + OH$	6.87×10^{13}	0	3.64
$O_2 + OH \rightarrow H + O_3$	4.40×10^{7}	1.4	329.44
$O_3 + OH \rightarrow HO_2 + O_2$	9.60×10^{11}	0	8.32
$O_3 + HO_2 \rightarrow OH + O_2 + O_2$	1.66×10^{11}	−0.3	8.32

rapidly with saturated hydrocarbons. The adapted mechanism allowed for accurate predictions of the laminar flame speed, temperature, and species profiles for C_3H_8 flames at a pressure of 101.3 kPa.

When the temperature, O, and O_3 concentration profiles were plotted, it became apparent that there was an increase in the temperature early in the pre-heat zone and a shifting of the overall temperature gradient (Fig. 10). The early pre-heat zone of the flame shows that a decrease in the O_3 concentration corresponds to an increase in the O concentration and the temperature profile.

A rate of production analysis was performed to understand the underlying flux of species and the overall enhancement mechanism. In Fig. 10, the results of a rate of production of O shows that upon O_3 decomposition because of the slightly elevated temperatures in the pre-heat zone, the O rapidly reacts with the fuel via the reactions

$$C_3H_8 + O \rightarrow n\text{-}C_3H_7 + OH \quad (8)$$

$$C_3H_8 + O \rightarrow iso\text{-}C_3H_7 + OH. \quad (9)$$

The two reactions of (8) and (9) provide the first key initiation steps in the extraction of chemical heat release by abstracting an H from the parent fuel to produce OH. Simultaneously, OH is also produced from the reaction of O_3 with H via

$$O_3 + H \rightarrow OH + O_2, \quad (10)$$

shown in Fig. 11. The rate constant for this reaction is shown in Table 2. Reactions (8)–(10) are important because they provide the OH necessary to react and form H_2O and heat release to enhance the flame speed. A rate of production of OH analysis is shown in Fig. 11 and identifies the major reaction pathways that change significantly in the early stages of the flame following O_3 decomposition. The three most important reactions are

$$CH_2O + OH \rightarrow HCO + H_2O \quad (11)$$

$$OH + HO_2 \rightarrow H_2O + O_2 \quad (12)$$

$$C_3H_8 + OH \rightarrow iso\text{-}C_3H_7 + H_2O. \quad (13)$$

While reactions (11)–(13) all form H_2O to produce heat release early in the flame, the two most important reactions are (11) and (12). A rate of production of heat release early in the pre-heat zone of the flame shows that reactions (11) and (12) are significant contributors of heat, which elevates the temperature. Fig. 12 shows the increased chemical heat release at lower temperatures with O_3 addition, with the most significant impact between 700 K and 1300 K. The elevated level of heat release earlier in the flame accelerates other reactions to change the structure of the flame, which in turn enhances the rate at which the flame can propagate. Furthermore, Fig. 12 shows that the peak heat release is higher with O_3 addition because of the additional energy that was coupled into the system by the plasma.

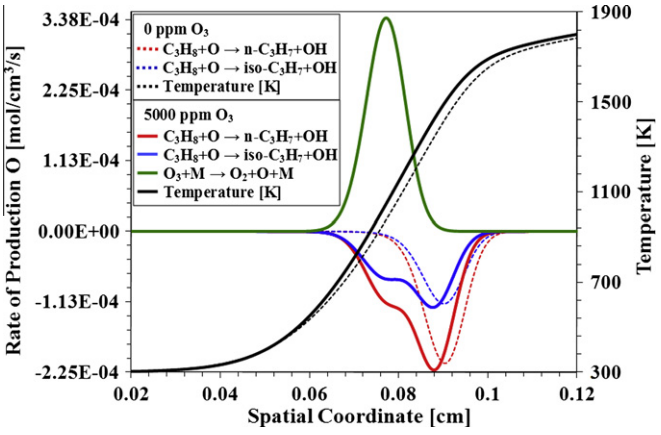

Fig. 10. Numerical simulation results showing the early rise in the temperature profile from chemical heat release and the rate of production of O with and without O_3 addition.

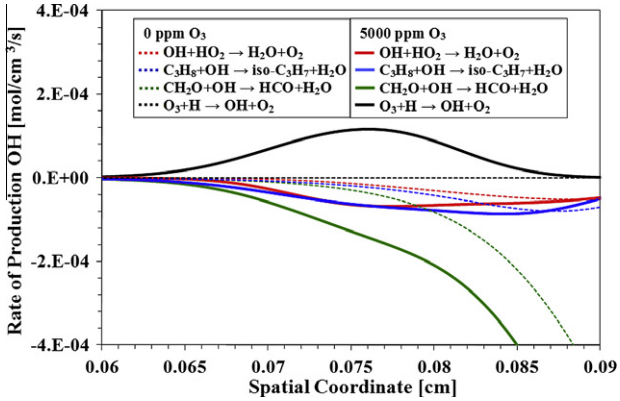

Fig. 11. Rate of production of OH showing the change of reaction pathways with O_3 addition to create stable products and heat release for flame speed enhancement.

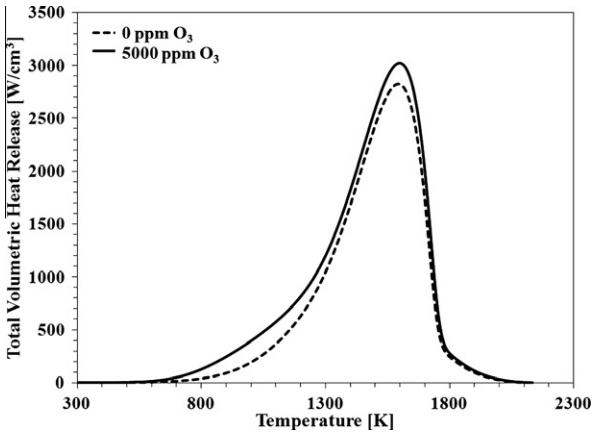

Fig. 12. Heat release versus temperature showing elevated levels of chemical heat release at lower temperatures with O_3 addition.

Therefore the enhancement scheme begins with the decomposition of O_3 by reaction (6) early in the pre-heat zone of the flame, releasing O which rapidly reacts with the parent fuel via reactions (8) and (9). The O_3 also reacts with H via reaction (10) to produce additional OH. The OH that is produced then reacts with the fuel and fuel fragments, such as CH_2O, to form H_2O and heat mostly via reactions (11) and (12) to elevate the temperatures. The elevated temperatures promote more rapid reactions early in the flame to enhance the flame propagation speed. The O_3 acts as a transporter of energy from the plasma to the early stages of the flame, in the pre-heat zone, where it seeds O into the flow to extract chemical heat release.

Furthermore, to demonstrate that the effect was not just simply the heat released after the decomposition of O_3 and recombination of O, a fictitious reaction was added to the mechanism to quench the O_3 to O_2 to extract all of the energy to the flow far upstream of the flame zone. This was accomplished by adding the reaction of

$$O_3 + O_3 \rightarrow O_2 + O_2 + O_2, \quad (14)$$

with a rate sufficiently fast to consume all of the O_3 far upstream of the flame front where the temperature was 300 K. The results of the flame speed enhancement with and without reaction (14) are shown in Fig. 13, along with the experimental data. It is shown

clearly that when O_3 quenches far upstream of the flame, the temperature only increases by several degrees to enhance the flame speed much less than when O_3 reaches the flame pre-heat zone. Therefore, when O_3 reaches the pre-heat zone of the flame, some chemical heat release is extracted to give significant flame speed enhancement. Furthermore, the results in Fig. 13 also shows the good agreement between the enhancements found in the experiments and in the computations when the O_3 reaches the pre-heat zone of the flame.

With the knowledge that O_3 addition to a lifted flame will significantly enhance flame propagation speed, it is of interest to take into account the efficiency of producing O_3. If one considers the production of O_3 in a dielectric barrier, which is the most common production method, there exists a critical concentration. If large amounts of power are supplied to the discharge to produce high concentrations of O, the recombination of O to O_2 becomes a significant pathway, competing with the O_3 production pathway of (6). For example, if a concentration of 1% O is produced, every second O atom recombines to O_2 instead of forming O_3. On the other hand, if the power of the discharge is too low, the energy loss to ions becomes increasingly important. A reasonable compromise is found when the dissociation in the plasma discharge reaches approximately 0.2% [54]. Therefore, with 0.2% (2000 ppm) of O_3, the kinetic enhancement of flame speed would be approximately 4%. With the addition of the changes in the flame front curvature caused by the kinetic enhancement, the overall flame speed would be enhanced between 10% and 15%. Therefore, in a practical system, the production and injection of O_3 in the cold transport to a flame can yield significant flame propagation enhancement with minimal energy expenditure.

4. Conclusions

A platform to study quantitatively the enhancement effects of plasma-produced O_3 on hydrocarbon flame speeds was developed. It was found that O_3 had significant kinetic enhancement effects on the propagation speeds of C_3H_8 lifted flames. The results showed that plasma-produced O_3 becomes a carrier of O at low temperatures. Since the lifetime of O is extremely short, especially at room temperature because of recombination and wall quenching reactions, the attachment of O to O_2 allows for extended cold transport of O. With temperatures lower than approximately 400 K, the O_3 can transport O atoms almost indefinitely to a reaction system. The only difference in enhancement will come from the energy required to break the bond of the weakly attached O in O_3, which requires much less energy than producing O from O_2. Numerical simulation results showed that O_3 decomposition and reaction with H in the pre-heat zone of the flame produced O and OH, respectively, from which the O reacted rapidly with the fuel to produce OH. The OH subsequently reacted with the fuel and fuel fragments, such as CH_2O, to form H_2O and accelerated fuel oxidation. The chemical heat release early in the pre-heat zone of the flame resulted in increased propagation speed of the flame.

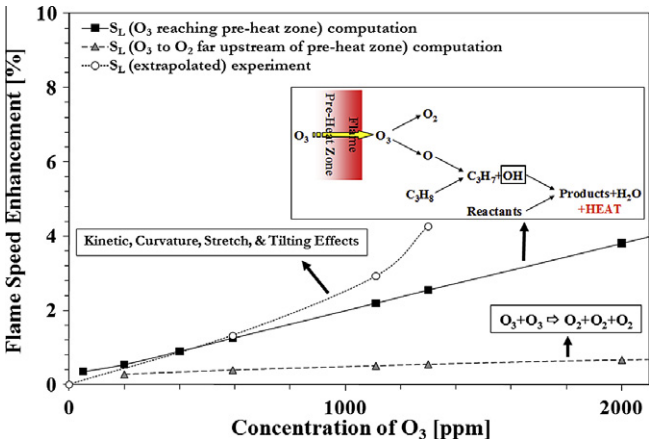

Fig. 13. Comparison plot of experimental results and numerical simulation results showing kinetic enhancement by O_3.

Equally as important was the coupling effect that the kinetic enhancement had on the hydrodynamics at the flame front. The fuel and velocity gradients at the premixed flame head create a unique triple flame front with curvature, stretch, and tilting relative to the flow. Because of the unique triple flame structure of lifted flames, the presence of O_3 at the flame front creates a kinetic enhancement which also induces hydrodynamic enhancement. The maximum overall flame speed enhancement in the laboratory coordinate was shown to be as high as 8% with 1260 ppm of O_3, while the enhancement locally was much lower at about 3%. When extrapolated to a zero mixture fraction gradient where the hydrodynamics of the flame were averaged and minimized, the enhancement was much more comparable to the pure kinetic enhancement at approximately 4%. The results indicate the very important finding that in a practical system where there are fuel and velocity gradients, stretch, curvature, tilting, and significant concentrations of O_3, the flame speed can be greatly enhanced.

Furthermore, the results of the current research imply that when energy is coupled into specific plasma-produced species, there is no requirement for the control of heat loss. For example, if energy is coupled into a reactive flow to raise the translational gas temperature only, there needs to be careful thermal management. Whereas, when energy is coupled into stable species, no thermal management needs to be considered for O_3 when the temperatures are below approximately 400 K. The energy contained within the species can be transported for significant distances and residence times and extracted at the combustion reaction zone.

Additionally, the results of the deposition of energy at a critical location in the early stages of the flame are vital since one of the most important parameters in plasma-assisted combustion is the characteristic time scales involved. Ozone addition illustrates the importance of time scales because if O_3 decomposes far upstream of the flame, the O released would recombine and not react with the fuel because the temperatures were not high enough to support the propagation of those reactions within the flow residence time to the flame. But when the O_3 decomposes and releases O to the reactants when the temperatures were only slightly elevated above the ambient, the fuel plus O reactions became dominant over recombination and quenching reactions. The chemical enthalpy that was extracted upstream of the flame stimulates other reactions as well as the diffusion of heat, enhancing the propagation of the flame. Therefore, the competition between the time scales of collisional quenching and reactive quenching is extremely critical when trying to achieve combustion enhancement through plasma activation.

Lastly, this work demonstrated another important step in developing an understanding of the most important plasma-produced species. With the knowledge of NO_x and O_3, less stable and shorter lifetime plasma-produced species can now be investigated more thoroughly. The results of O_3 enhancement of flame propagation speed provided here gives a firm foundation since O_3 will always exist in an oxygen containing plasma. Therefore, the pursuit of shorter lifetime excited oxygen species, such as $O_2(a^1\Delta_g)$, can be pursued. The results of the effects of $O_2(a^1\Delta_g)$ on flame propagation speed using a lifted flame apparatus at reduced pressures are discussed in part II of this investigation.

Acknowledgments

This work was supported by the Air Force Office of Scientific Research with grant number FA9550-07-1-0136 and the AFOSR MURI

research grant on plasma-assisted combustion under the technical monitor of program manager Dr. Julian Tishkoff. Part of the research was performed while the corresponding author held a National Research Council Research Associateship Award at the United States Air Force Research Laboratory, Wright-Patterson Air Force Base. The authors wish to thank Mr. Dmitry Opaits for his expertise and help with the ozone generation and Dr. Campbell Carter for insightful discussions.

References

[1] H. Beach, E. Mackley, R. Rogers, W. Chinitz, in: 17th JANNAF Combustion Meeting, vol. 329, 1980. pp. 639–659.
[2] M. Gerstein, P. Choudhury, J. Prop. Power 1 (5) (1985) 399–402.
[3] T. Helfrich, F. Schauer, R. Bradley, J. Hoke, in: 45th AIAA Aerospace Sciences Meeting, vol. 4, 2007. pp. 2755–2767.
[4] Y. Ju, T. Niioka, Combust. Flame 102 (4) (1995) 462–470.
[5] S. Tabejamaat, Y. Ju, T. Niioka, AIAA J. 35 (9) (1997) 1441–1447.
[6] E. Barbi, J. Mahan, W. O'Brien, T. Wagner, J. Prop. Power 5 (2) (1989) 129–133.
[7] I. Kimura, H. Aoki, M. Kato, Combust. Flame 42 (1981) 297–305.
[8] K. Takita, A. Moriwaki, T. Kitagawa, G. Masuya, Combust. Flame 132 (4) (2003) 679–689.
[9] T. Wagner, W. O'Brien, G.E. Northam, J. Prop. Power 5 (5) (1989) 548–554.
[10] T. Ombrello, Y. Ju, IEEE Trans. Plasma Sci. 36 (6) (2008) 2924–2932.
[11] T. Ombrello, Y. Ju, A. Fridman, AIAA J. 46 (10) (2008) 2424–2433.
[12] T. Ombrello, X. Qin, Y. Ju, A. Gutsol, A. Fridman, AIAA J. 44 (1) (2006) 142–150.
[13] S. Bozhenkov, S. Starikovskaia, A.Y. Starikovskii, Combust. Flame 133 (2003) 133–146.
[14] A. Starikovskii, Proc. Combust. Inst. 30 (2005) 2405–2417.
[15] G. Lou, A. Bao, M. Nishihara, S. Keshav, Y. Utkin, J. Rich, W. Lempert, I. Adamovich, Proc. Combust. Inst. 31 (2007) 3327–3334.
[16] S. Pancheshnyi, D. Lacoste, A. Bourbon, C. Laux, IEEE Trans. Plasma Sci. 34 (6) (2006) 2478–2487.
[17] H. Jagers, A. Von Engel, Combust. Flame 16 (1971) 275–285.
[18] S. Won, M. Cha, C. Park, S. Chung, Proc. Combust. Inst. 31 (2007) 963–970.
[19] S. Won, S. Ryu, M. Kim, M. Cha, S. Chung, Combust. Flame 152 (2008) 496–506.
[20] I. Esakov, L. Grachev, K. Khodatev, V. Vinogradov, D. Van Wie, in: 44th AIAA Aerospace Sciences Meeting and Exhibit, AIAA-2006-1212, 2006.
[21] Y. Ju, S. Macheret, R. Miles, D. Sullivan, in: 40th AIAA/ASME/SAE/ASEE Joint Propulsion Conference and Exhibit, AIAA-2004-2721, 2004.
[22] S. Zaidi, S. Macheret, L. Vasilyak, R. Miles, Y. Ju, D. Sullivan, in: 35th AIAA Plasmadynamics and Lasers Conference, AIAA-2004-3707, 2004.
[23] E. Stockman, S. Zaidi, R. Miles, C. Carter, M. Ryan, Combust. Flame 156 (2009) 1453–1461.
[24] C. Cathey, J. Cain, H. Wang, M. Gunderson, C. Carter, M. Ryan, Combust. Flame 154 (2008) 715–727.
[25] I. Kosarev, N. Aleksandrov, S. Kindysheva, S. Starikovskaia, A. Starikovskii, J. Prop. Power 24 (6) (2008) 1182–1197.
[26] S. Starikovskaia, J. Phys. D: Appl. Phys. 39 (2006) R265–R299.
[27] B. Gordiets, C. Ferreira, V. Guerra, J. Loureiro, J. Nahorny, D. Pagnon, M. Touzeau, M. Vialle, IEEE Trans. Plasma Sci. 23 (4) (1995) 750–768.
[28] M. Uddi, N. Jiang, E. Mintusov, I. Adamovich, W. Lempert, Proc. Combust. Inst. 32 (2009) 929–936.
[29] A.A. Ionin, I.V. Kochetov, A.P. Napartovich, N.N. Yuryshev, J. Phys. D: Appl. Phys. 40 (2007) R25–R61.
[30] V. Golovitchev, J. Chomiak, Combust. Sci. Technol. 135 (1–6) (1998) 31–47.
[31] H. Nishida, T. Tachibana, J. Prop. Power 22 (1) (2006) 151–157.
[32] T. Nomaguchi, S. Koda, Proc. Combust. Inst. 22 (1) (1988) 1677–1682.
[33] T. Tachibana, H. K, H. Nishida, H. Osada, Combust. Flame 85 (3–4) (1991) 515–519.
[34] H. Yamada, M. Yoshii, A. Tezaki, Proc. Combust. Inst. 30 (1) (2005) 2773–2780.
[35] D. Lucas, D. Dunn-Rankin, K. Hom, N. Brown, Combust. Flame 69 (2) (1987) 171–184.
[36] B. Lukhovitskii, A. Starik, N. Titova, Combust. Explor. Shock Waves 41 (4) (2005) 386–394.
[37] A. Starik, B. Lukhovitsky, N. Titova, J. Russ. Laser Res. 27 (6) (2006) 533–551.
[38] M. Gluckstein, R. Morrison, T. Khammash, Combustion with Ozone-Modification of Flame Speeds C_2 Hydrocarbon–Air Mixtures, University of Michigan, 1955.
[39] R. Atkinson, D.L. Baulch, R.A. Cox, J.N. Crowley, R.F. Hampson, R.G. Hynes, M.E. Jenkin, M.J. Rossi, J. Troe, Atm. Chem. Phys. 4 (2004) 1461–1738.
[40] D.S. Stafford, M.J. Kushner, J. Appl. Phys. 96 (2004) 2451–2465.
[41] K.H. Becker, W. Groth, U. Schurath, Chem. Phys. Lett. 8 (1971) 259–262.
[42] J. Malicet, D. Daumont, J. Charbonnier, C. Parisse, A. Chakir, J. Brion, J. Atm. Chem. 21 (3) (1995) 263–273.
[43] S. Chung, Proc. Combust. Inst. 31 (1) (2007) 877–892.
[44] J. Lee, S. Won, S. Jin, S. Chung, Combust. Flame 135 (4) (2003) 449–462.
[45] Y. Ju, Y. Xue, Proc. Combust. Inst. 30 (2005) 295–301.
[46] Y. Xue, Y. Ju, Combust. Sci. Technol. 178 (2006) 2219–2247.
[47] M. Kim, S. Won, S. Chung, Proc. Combust. Inst. 31 (2007) 901–908.
[48] G. Ruetsch, L. Vervisch, A. Linan, Phys. Fluids 7 (1995) 1447–1454.
[49] PREMIX from the CHEMKIN Package, Reaction Design, 6440 Lusk Boulevard, Suite D-205 San Diego, CA 92121. <http://www.reactiondesign.com>.
[50] L. Ibraguimova, G. Smekhov, O. Shatalov, Recommended Rate Constants of Chemical Reactions in an H_2–O_2 Gas Mixture with Electronically Excited Species $O_2(^1\Delta)$, $O(^1D)$, $OH(^2\Sigma)$ Involved, Institute of Mechanics of Lomonosov, Moscow State University, 2003.
[51] G. Smekhov, L. Ibraguimova, S. Karkach, O. Skrebkov, O. Shatalov, High Temp. 45 (3) (2007) 395–407.
[52] Z. Qin, V. Lissianski, H. Yang, W. Gardiner, S. Davis, H. Wang, Proc. Combust. Inst. 28 (2) (2000) 1663–1669.
[53] R. Morrissey, C. Schubert, Combust. Flame 7 (3) (1963) 263–268.
[54] U. Kogelschatz, B. Eliasson, W. Egli, J. Phys. IV 7 (C4) (1997) 47–66.